AIAA JOURNAL
Vol. 37, No. 9, September 1999

Nonlinear Flutter of Composite Panels Under Yawed Supersonic Flow Using Finite Elements

K. Abdel-Motaglay,* R. Chen,† and C. Mei‡
Old Dominion University, Norfolk, Virginia 23529-0247

A finite element formulation is presented for the effects of arbitrary flow direction on the large-amplitude supersonic flutter of composite panels. The von Kármán large-deflection plate theory is used to account for large-amplitude limit-cycle oscillations, quasisteady first-order piston theory aerodynamics is employed for aerodynamic loading, and first-order shear deformation theory is used for laminated composite panels. An efficient solution procedure is presented by using the modal transformation to reduce the number of nonlinear panel flutter equations and then applying the linearized updated mode with nonlinear time function approximation to the reduced nonlinear panel flutter modal equations. A modal participation is defined and the minimum number of linear modes for accurate and converged limit-cycle response can be ensured. Examples are given for isotropic and composite panels at yawed supersonic flow.

Nomenclature

$[A]$, $[B]$, $[D]$, $[A_s]$	= extension, coupling, bending, and shear laminate stiffness matrices
$[A_x]$, $[A_y]$	= aerodynamic influence matrices
a, b	= panel dimensions
$[G]$	= aerodynamic damping matrix
g_a	= aerodynamic damping
h	= panel thickness
$[K]$	= system linear stiffness matrix
$[K1]$	= first-order nonlinear system stiffness matrix
$[K2]$	= second-order nonlinear system stiffness matrix
$[M]$	= system mass matrix
M_∞	= freestream Mach number
$\{\boldsymbol{q}\}$	= modal coordinate vector
q_a	= dynamic pressure
u, v	= in-plane displacements
V_∞	= freestream air velocity
w	= panel deflection
$\{\varepsilon^o\}$	= in-plane strain vector
$\{\boldsymbol{\kappa}\}$	= curvature vector
Λ	= flow yaw angle
λ	= nondimensional dynamic pressure
ρ	= plate mass density
ρ_a	= air mass density
ψ_x, ψ_y	= rotations of the normal about x and y axes
ω_o	= reference frequency

I. Introduction

THE effects of flow yawing on the critical flutter dynamic pressure on isotropic and orthotropic rectangular panels at supersonic speeds were investigated during the late sixties and early seventies. Kordes and Noll[1] and Bohon[2] studied analytically the influence of arbitrary flow angles on isotropic and orthotropic rectangular panels with classical simply supported boundary conditions. Durvasula[3,4] used the Rayleigh–Ritz method and 16-term beam functions to study the flow yawing and plate obliquity effects of simply supported and clamped rectangular isotropic panels. Kariappa et al.[5] and Sander et al.[6] used the finite element method (FEM) to study the effects of flow yawing of isotropic parallelogram panels. Shyprykevich and Sawyer[7] and Sawyer[8] have shown experimentally and theoretically that critical dynamic pressure is dependent on flow angle and flexible supports. They found that orthotropic panels mounted on flexible supports experienced large reductions in critical flutter dynamic pressure for only small changes in flow angle. An excellent review of the FEM applied to linear models of supersonic aeroelastic stability of plates and shells is given by Bismarck-Nasr.[9]

Linear structure theory can predict the critical flutter dynamic pressure and the frequency of vibration. When the panel amplitude of vibration gets large, the effect of in-plane stretching on panel behavior becomes significant. These in-plane forces tend to restrain panel motion so that bounded limit-cycle oscillations (LCOs) are observed. The amplitude of the LCOs grows as the dynamic pressure increases. The existence of LCOs implies that large-deflection nonlinear structural theory should be used. Use of the nonlinear structural theory will yield panel deflection and stresses and thus panel fatigue life can be estimated.[10,11] An excellent survey on nonlinear panel flutter through 1970 is given by Dowell.[12] Gray and Mei[13] give a survey of various theoretical considerations and analytical methods for nonlinear panel flutter up to 1991. Various analytical approaches, including the FEM for nonlinear panel flutter at supersonic speeds, have been reviewed by Zhou et al.[14] An exhaustive search of the literature reveals that few investigations on nonlinear panel flutter have considered the effects of flow yawing. Friedmann and Hanin[15] used first-order piston theory aerodynamics and Galerkin's method in the spatial domain; they then solved the reduced coupled nonlinear ordinary differential modal equations with numerical integration. Using a 4×2 mode model—four natural (in vacuo) modes in the x direction and two modes in the y direction—they obtained LCOs for simply supported isotropic and orthotropic rectangular panels. Chandiramani et al.[16] used third-order piston theory aerodynamics and Galerkin's method in the spatial domain. They solved the reduced coupled nonlinear ordinary differential modal equations using a predictor and a Newton–Raphson-type corrector technique for limit-cycle periodic solutions. They employed direct numerical integration for nonperiodic and chaotic solutions and used a 2×2 mode model—two natural modes in the x and y directions—for simply supported rectangular laminated panels. However, with the development of high-speed flight vehicles, such as the High-Speed Civil Transport, the X-33 Advanced Technology Demonstrator, the Reusable Launch Vehicle, the Joint Strike Fighter, and the X-38 Technology Demonstrator using a lifting-body concept, currently under way, the capability for analyzing nonlinear panel flutter of composite panels at arbitrary yawed supersonic flow is needed urgently.

This paper presents a finite element formulation and an efficient solution procedure for analysis of supersonic nonlinear flutter

Received 8 April 1998; revision received 20 January 1999; accepted for publication 9 March 1999.

*Graduate Research Assistant, Department of Aerospace Engineering. Student Member AIAA.
†Research Associate, Department of Aerospace Engineering.
‡Professor, Department of Aerospace Engineering. Associate Fellow AIAA.

of composite panels with arbitrary flow direction. First, the finite element nonlinear panel flutter equations are formulated in the structural-node degrees of freedom (DOF). Then, the number of equations is reduced using a modal transformation. The minimum number of linear natural modes needed for an accurate and converged LCO flutter response can be ensured from the modal participation values. The reduced nonlinear modal equations are solved using the linearized updated mode with nonlinear time function (LUM/NTF)[11,13] approximation with an efficient real and complex eigensolver.[17,18] The solution procedure is efficient and has a great advantage in computation time. Examples of isotropic and composite panels at yawed supersonic flow are given.

II. Finite Element Formulation

A. Equations in Structure-Node DOF

The in-plane strains, curvatures, and shear strains based on von Kármán large deflection and first-order shear deformation theory for laminated composite plates are given by

$$\{\varepsilon^o\} = \{\varepsilon^o_m\} + \{\varepsilon^o_b\} = \begin{Bmatrix} u_{,x} \\ v_{,y} \\ u_{,y} + v_{,x} \end{Bmatrix} + \frac{1}{2}\begin{Bmatrix} w^2_{,x} \\ w^2_{,y} \\ 2w_{,x}\, w_{,y} \end{Bmatrix}$$

$$\{\kappa\} = \begin{Bmatrix} \psi_{y,x} \\ \psi_{x,y} \\ \psi_{y,y} + \psi_{x,x} \end{Bmatrix}, \qquad \{\gamma\} = \begin{Bmatrix} w_{,y} + \psi_x \\ w_{,x} + \psi_y \end{Bmatrix} \tag{1}$$

where the subscripts m and b denote membrane (in-plane) and bending components, respectively. The constitutive relations for a composite laminate expressed in stress resultants are

$$\begin{Bmatrix} N \\ M \end{Bmatrix} = \begin{bmatrix} A & B \\ B & D \end{bmatrix}\begin{Bmatrix} \varepsilon^o \\ \kappa \end{Bmatrix}, \qquad \{R\} = [A_s]\{\gamma\} \tag{2}$$

Quasisteady first-order piston theory aerodynamics is employed for the aerodynamic pressure. Although this theory neglects the effects of three-dimensional and flow memory, it gives a very satisfactory approximation for high supersonic Mach numbers ($M_\infty > 1.6$). The aerodynamic pressure is given by

$$\Delta p = -\frac{2q_a}{\beta}\left(w_{,x}\cos\Lambda + w_{,y}\sin\Lambda + \frac{M^2_\infty - 2}{M^2_\infty - 1}\frac{1}{V_\infty}w_{,t}\right) \tag{3}$$

where $q_a = \rho_a V^2_\infty/2$, $\beta = \sqrt{(M^2_\infty - 1)}$, and Λ is the flow yaw angle with the x axis. Using Hamilton's principle and finite element expressions, we can express the element equations of motion for nonlinear panel flutter at an arbitrary flow yawing angle as

$$\frac{1}{\omega^2_o}\begin{bmatrix} [m]_b & 0 \\ 0 & [m]_m \end{bmatrix}\begin{Bmatrix} \ddot{w}_b \\ \ddot{w}_m \end{Bmatrix} + \frac{g_a}{\omega_o}\begin{bmatrix} [g] & 0 \\ 0 & 0 \end{bmatrix}\begin{Bmatrix} \dot{w}_b \\ \dot{w}_m \end{Bmatrix}$$
$$+\left(\lambda\begin{bmatrix} [a_x]\cos\Lambda + [a_y]\sin\Lambda & 0 \\ 0 & 0 \end{bmatrix} + \begin{bmatrix} [k]_b & [k_B] \\ [k_B]^T & [k]_m \end{bmatrix}\right.$$
$$+\begin{bmatrix} \alpha_s[k_s] & 0 \\ 0 & 0 \end{bmatrix} + \begin{bmatrix} [k1_B] + [k1_{Nm}] + [k1_{Nb}] & [k1]_{bm} \\ [k1]_{mb} & 0 \end{bmatrix}$$
$$\left.+\begin{bmatrix} [k2] & 0 \\ 0 & 0 \end{bmatrix}\right)\begin{Bmatrix} w_b \\ w_m \end{Bmatrix} = \begin{Bmatrix} 0 \\ 0 \end{Bmatrix} \tag{4}$$

where $\omega_o = (D_{110}/\rho h a^4)^{1/2}$ is a reference frequency, α_s is the shear correction factor, and D_{110} is the first entry in laminate bending rigidity $[D]$. The subscripts B, s, Nm, and Nb denote that the corresponding stiffness matrix is due to the laminate extension bending stiffness $[B]$, transverse shear deformation, and membrane force components $\{N_m\}(=[A]\{\varepsilon^o_m\})$ and $\{N_b\}(=[B]\{\kappa\})$, respectively; subscripts x and y denote that the corresponding aerodynamic influence matrix is due to the $w_{,x}$ and $w_{,y}$ terms, respectively, in Eq. (3). The nondimensional dynamic pressure λ and the aerodynamic damping g_a are given by

$$\lambda = \frac{2q_a a^3}{\beta D_{110}}, \qquad g_a = \sqrt{\lambda C_a} \tag{5}$$

where $C_a = \mu(M^2_\infty - 2)^2/\beta(M^2_\infty - 1)^2$ and $\mu = \rho_a a/\rho h$. For $M_\infty \gg 1$, $C_a \approx \mu/M_\infty$.

Assembling the element matrices and considering the kinematic boundary conditions, we can write the system equations in structure-node DOF as

$$\frac{1}{\omega^2_o}\begin{bmatrix} [M]_b & 0 \\ 0 & [M]_m \end{bmatrix}\begin{Bmatrix} \ddot{W}_b \\ \ddot{W}_m \end{Bmatrix} + \frac{g_a}{\omega_o}\begin{bmatrix} [G] & 0 \\ 0 & 0 \end{bmatrix}\begin{Bmatrix} \dot{W}_b \\ \dot{W}_m \end{Bmatrix}$$
$$+\left(\lambda\begin{bmatrix} [A_x]\cos\Lambda + [A_y]\sin\Lambda & 0 \\ 0 & 0 \end{bmatrix}\right.$$
$$+\begin{bmatrix} [K]_b + [K_s] & [K_B] \\ [K_B]^T & [K]_m \end{bmatrix}$$
$$+\begin{bmatrix} [K1_B] + [K1_{Nm}] + [K1_{Nb}] & [K1]_{bm} \\ [K1]_{mb} & 0 \end{bmatrix}$$
$$\left.+\begin{bmatrix} [K2] & 0 \\ 0 & 0 \end{bmatrix}\right)\begin{Bmatrix} W_b \\ W_m \end{Bmatrix} = \begin{Bmatrix} 0 \\ 0 \end{Bmatrix} \tag{6}$$

where $[A_x]$ and $[A_y]$ are the aerodynamic influence matrices and $[K1]$ and $[K2]$ depend linearly and quadratically on the unknown displacements $\{W\}$.

By neglecting the in-plane inertia term in Eq. (6), the in-plane displacements can be expressed in terms of the bending displacement as

$$\{W_m\} = -[K]^{-1}_m\left([K_B]^T + [K1]_{mb}\right)\{W_b\} \tag{7}$$

and the system equations (6) are expressed in terms of the bending displacement $\{W_b\}$ as

$$\left(1/\omega^2_o\right)[M_b]\{\ddot{W}_b\} + (g_a/\omega_o)[G]\{\dot{W}_b\} + ([K_L] + [K_{NL}])\{W_b\} = \{0\} \tag{8}$$

where the linear and nonlinear stiffness matrices are given by

$$[K_L] = \lambda([A_x]\cos\Lambda + [A_y]\sin\Lambda) + [K]_b + [K_s] - [K_B][K]^{-1}_m[K_B]^T \tag{9}$$

$$[K_{NL}] = -[K_B][K]^{-1}_m[K1]_{mb} + [K1_B] + [K1_{Nm}] + [K1_{Nb}] + [K2] - [K1]_{bm}[K_m]^{-1}\left([K_B]^T + [K1]_{mb}\right) \tag{10}$$

Equation (8) can be solved for nonlinear flutter response in the frequency domain using the LUM/NTF approximation.[11,13] However, use of the LUM/NTF approach to the system equations in the form presented in Eq. (8) has two disadvantages: 1) The element nonlinear stiffness matrices have to be evaluated and the system nonlinear stiffness $[K_{NL}]$ must be assembled and updated at each iteration, and 2) the number of structure-node DOF of $\{W_b\}$ is usually very large. This turned out to be computationally costly.

An efficient solution procedure, presented here for the first time, is to transfer Eq. (8) into the modal coordinates with a modal truncation. Based on the values of modal participation, the number of the nonlinear panel flutter modal equations is kept at a minimum. The LUM/NTF method then is applied to the reduced modal equations. The solution procedure is described in the following section.

B. Equations in Modal Coordinates

Assuming that the panel deflection can be expressed as a linear combination of some known functions as

$$\{W_b\} = \sum_{r=1}^{n} q_r(t)\{\phi_r\} = [\Phi]\{q\} \tag{11}$$

where the number of retained linear (in vacuo) modes, n, is much smaller than the number of structure bending-node DOF in bending, $\{W_b\}$. The normal mode $\{\phi_r\}$, which is normalized with the maximum component to unity, and the linear natural frequency ω_r are obtained from the linear vibration of the system:

$$\left(\omega_r^2/\omega_o^2\right)[M]_b\{\phi_r\} = \left([K]_b + [K_s] - [K_B][K]_m^{-1}[K_B]^T\right)\{\phi_r\} \tag{12}$$

Because matrices $[K1]_{mb}$, $[K1_B]$, $[K1_{Nb}]$, and $[K2]$ are all functions of the unknown bending DOF $\{W_b\}$, they can be expressed as the sum of products of modal coordinates and nonlinear modal stiffness matrices as

$$\left([K1]_{mb}, [K1_B], [K1_{Nb}]\right) = \sum_{r=1}^{n} q_r\left([K1]_{mb}^{(r)}, [K1_B]^{(r)}, [K1_{Nb}]^{(r)}\right)$$

$$[K2] = \sum_{r=1}^{n}\sum_{s=1}^{n} q_r q_s [K2]^{(rs)} \tag{13}$$

where the superindices of those nonlinear modal stiffness matrices denote that they are assembled from the corresponding element nonlinear stiffness matrices. Those element nonlinear stiffness matrices are evaluated with the corresponding element components $\{w\}_b^{(r)}$ obtained from the known system linear mode $\{\phi_r\}$. Therefore, those nonlinear modal stiffness matrices are constant matrices. The first-order nonlinear stiffness matrix $[K1_{Nm}]$ is a linear function of the in-plane displacement $\{W_m\}$, and from Eq. (7), $\{W_m\}$ consists of two terms:

$$\{W\}_m = -[K]_m^{-1}[K_B]^T[\Phi]\{q\} - [K]_m^{-1}\left(\sum_{r=1}^{n} q_r[K1]_{mb}^{(r)}\right)[\Phi]\{q\}$$

$$= -\sum_{r=1}^{n} q_r\{\phi_r\}_m - \sum_{r=1}^{n}\sum_{s=1}^{n} q_r q_s\{\phi_{rs}\}_m \tag{14}$$

where the two in-plane modes corresponding to the rth bending mode $\{\phi_r\}$ are given as

$$\{\phi_r\}_m = [K]_m^{-1}[K_B]^T\{\phi_r\}$$

$$\{\phi_{rs}\}_m = [K]_m^{-1}[K1]_{mb}^{(r)}\{\phi_s\} \tag{15}$$

Thus, the nonlinear stiffness matrix $[K1_{Nm}]$ can be expressed as the sum of two nonlinear modal stiffness matrices:

$$[K1_{Nm}] = -\sum_{r=1}^{n} q_r[K1_{Nm}]^{(r)} - \sum_{r=1}^{n}\sum_{s=1}^{n} q_r q_s[K2_{Nm}]^{(rs)} \tag{16}$$

The nonlinear modal stiffness matrices $[K1_{Nm}]^{(r)}$ and $[K2_{Nm}]^{(rs)}$ are assembled and valuated with known in-plane modes $\{\phi_r\}_m$ and $\{\phi_{rs}\}_m$, respectively; they are also constant matrices. Equation (8) is transformed to the following reduced nonlinear system in the modal coordinates:

$$\left(1/\omega_o^2\right)[\bar{M}_b]\{\ddot{q}\} + (g_a/\omega_o)[\bar{G}]\{\dot{q}\} + ([\bar{K}_L] + [K_q] + [K_{qq}])\{q\} = \{0\} \tag{17}$$

where the modal matrices are given by

$$([\bar{M}_b], [\bar{G}], [\bar{K}_L]) = [\Phi]^T([M]_b, [G], [K_L])[\Phi] \tag{18}$$

and the quadratic and cubic terms in modal coordinates are

$$[K_q] = [\Phi]^T\sum_{r=1}^{n} q_r\big(-[K_B][K]_m^{-1}[K1]_{mb}^{(r)} + [K1_B]^{(r)} - [K1_{Nm}]^r$$

$$+ [K1_{Nb}]^{(r)} - [K1]_{bm}^{(r)}[K]_m^{-1}[K_B]^T\big)[\Phi] \tag{19}$$

$$[K_{qq}] = [\Phi]^T\sum_{r=1}^{n}\sum_{s=1}^{n} q_r q_s\big([K2]^{(rs)}$$

$$- [K2_{Nm}]^{(rs)} - [K1]_{bm}^{(r)}[K]_m^{-1}[K1]_{mb}^{(s)}\big)[\Phi] \tag{20}$$

All of the submatrices of Eq. (17) are defined in Eqs. (8–10), (13), and (16).

C. Solution Procedure

Now, the LUM/NTF approximation is used on the reduced nonlinear modal equation (17). The advantages are as follows: 1) There is no need to assemble and update the nonlinear stiffness matrices at each iteration because all nonlinear modal matrices are constant, and 2) the number of modal equations is much smaller. Also, the few influential modes to be kept can be determined by the modal participation value, which is defined as

$$\text{Participation of the } r\text{th mode} = \frac{\max|q_r|}{\sum_{s=1}^{n}|q_s|} \tag{21}$$

In addition, a power iterative nonlinear eigensolver, which can efficiently and accurately solve nonsymmetric equations to obtain real or complex eigenvalues and eigenvectors, introduced by Xue et al.,[17,18] can be employed to further reduce computational time. Application of the LUM/NTF approach to finite element nonlinear supersonic and hypersonic panel flutter has been documented widely; readers are referred to Refs. 10, 11, 13, 17, and 18. The solution procedure follows:

Given $W_{\max}$,

1) Assume $\{q\} = \{q_o\}e^{\Omega t} = \{q\}e^{(\alpha+i\omega)t}$.

2) For a given λ, solve the linearized eigenequation for the jth iteration:

$$\kappa_j[\bar{M}_b]\{q_o\}_j = ([\bar{K}_L] + [\bar{K}_{NL}])\{q_o\}_j$$

where

$$\kappa = -(\Omega/\omega_o)^2 - g_a(\Omega/\omega_o)$$

and

$$[\bar{K}_{NL}] = \tfrac{\sqrt{2}}{2}[K_q(\{q_o\}_{j-1})] + \tfrac{3}{4}[K_{qq}(\{q_o\}_{j-1})]$$

$[K_q]$ and $[K_{qq}]$ are defined in Eqs. (19) and (20), and $\{q_o\}_j$ is the updated modal solution.

3) Get $\{W_b\}$ from $\{q\}_j$ using $\{W_b\} = [\Phi]\{q_o\}_j$ and find $W_{\max_j}$.

Then adjust $\{q_o\}_j$ to result in the required $W_{\max}$:

$$\{q_o\}_j = \{q_o\}_j\frac{(W_{\max})_{\text{given}}}{W_{\max_j}}$$

4) Test for convergence of $\{q_o\}$; if no convergence, go to step 2.

5) Check for coalescence. If no coalescence, $\lambda = \lambda + \Delta\lambda$, then go to step 2.

III. Examples and Discussion

The nonlinear panel flutter equations developed in Eqs. (6) and (17) are general in the sense that they are applicable for either rectangular[13] or triangular[11] finite elements. The element employed in the examples is the three node triangular Mindlin (MIN3) plate element with improved transverse shear. The mass and linear stiffness matrices of the MIN3 element were developed by Tessler and Hughes,[19] and the shear correction factor is defined as

$$\alpha_s = 1\Big/\left(1 + 0.5\sum_{i=4,9} k_{sii}\Big/\sum_{i=4,9} k_{bii}\right)$$

The nonlinear stiffness matrices for the MIN3 element were developed by Chen and are given in detail in Ref. 20. The element aerodynamic matrices are given in the Appendix. The MIN3 element has 15 DOF, 5 at each apex node; the bending-node DOF, $\{w_b\}$, comprise transverse displacements and normal rotations w, ψ_x, and ψ_y; and the in-plane–node DOF, $\{w_m\}$, comprise u and v. Validation

Table 1 Modal participation values at various limit-cycle amplitudes for a simply supported square isotropic panel at 0-deg flow angle

	Modal participation, %					
$w_{\max}/h$	q_{11}	q_{21}	q_{31}	q_{41}	q_{51}	q_{61}
0.01	32.83	39.27	23.89	3.87	0.09	0.05
0.4	34.77	38.39	22.85	3.82	0.133	0.04
0.8	37.59	37.20	21.19	3.76	0.25	0.01

Table 2 Modal participation values at various limit-cycle amplitudes for a simply supported square isotropic panel at 45-deg flow angle

	Modal participation, %															
w_{max}/h	q_{11}	q_{21}	q_{12}	q_{22}	q_{31}	q_{13}	q_{32}	q_{23}	q_{41}	q_{14}	q_{33}	q_{42}	q_{24}	q_{43}	q_{34}	q_{44}
0.01	22.10	21.66	16.67	14.62	8.44	7.14	2.06	0.84	1.29	2.16	0.73	0.58	0.81	0.20	0.61	0.09
0.4	22.53	21.65	16.69	14.05	8.47	7.25	1.86	0.77	1.38	2.35	0.62	0.59	0.83	0.19	0.66	0.10
0.8	24.34	21.32	16.78	12.29	8.42	7.50	1.32	0.58	1.63	2.90	0.39	0.60	0.86	0.18	0.77	0.12

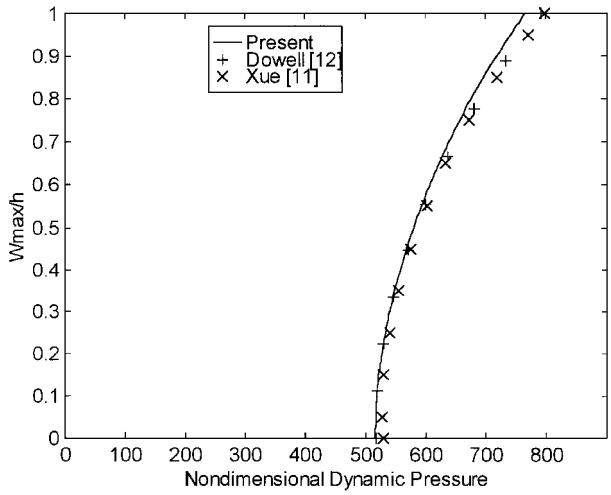

Fig. 1 Comparison of limit-cycle amplitude for a simply supported square isotropic panel.

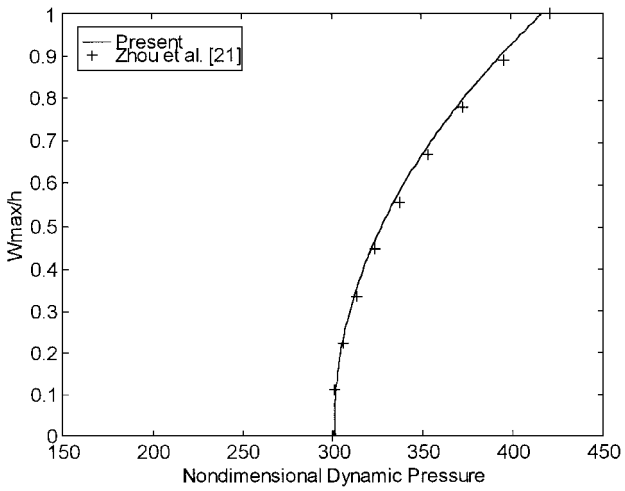

Fig. 2 Comparison of limit-cycle amplitude for a simply supported [0/45/− 45/90]$_s$ graphite/epoxy panel.

of the present FEM and the efficient solution procedure for limit-cycle results with other computations is given first. Then, effects of flow direction on nonlinear flutter are demonstrated by examples of rectangular isotropic and composite panels with yawed supersonic flow.

A. Validation

To validate the present finite element modal formulation, the limit-cycle results for square isotropic and composite panels are obtained and compared with other computations.

The LCO response for a simply supported square isotropic panel at $\Lambda = 0$ deg using a 10×10 mesh and a six-mode model is shown in Fig. 1. Limit-cycle results obtained by Dowell[12] using a six-mode model with Galerkin's method and numerical integration, and by Xue[11] using the finite element frequency-domain approach and 48 discrete Kirchoff triangular elements ($8 \times 3 \times 2$ mesh for half-plate model), also are shown in Fig. 1 for comparison. The present formulation is in good agreement with these two methods.

Table 3 Nondimensional dynamic pressure at various limit-cycle amplitudes for a simply supported square isotropic panel using different numbers of modes at 0- and 45-deg flow angles

Flow angle Λ	No. of modes, n	Dynamic pressure λ at w_{max}/h		
		0.01	0.4	0.8
0	2	393	419	475
	4	518	558	669
	6	518	558	669
45	5	522	561	660
	10	549	592	718
	15	559	603	739
	20	560	604	742
	25	559	603	740

For validation of the MIN3 element and the present finite element formulation for composite panels, the limit-cycle results of a simply supported eight-layered [0/45/−45/90]$_s$ graphite/epoxy square $30.5 \times 30.5 \times 0.127$ cm ($12 \times 12 \times 0.050$ in.) panel obtained by Zhou et al.[21] are compared with those obtained using the present formulation. The C^1 conforming rectangular plate bending element and the finite element time-domain modal formulation were employed in Ref. 21. The complete plate is modeled with 10×10 mesh or 200 MIN3 elements and a 16-mode model. The LCO response at $\Lambda = 0$ deg, shown in Fig. 2, clearly demonstrates the accuracy of the MIN3 element and the present finite element formulation.

B. Isotropic Panels

A simply supported square isotropic panel with immovable in-plane edges ($u = v = 0$) at flow angles $\Lambda = 0$ and 45 deg is studied in detail for modal convergence. The panel is modeled using a 10×10 mesh or 200 MIN3 elements. The number of structure DOF $\{W\}_b$ is of 279 for the system equations (8), and it is reduced to the modal coordinates to include the selected n modes. The modal participation values for three limit-cycle amplitudes $w_{max}/h = 0.01, 0.4$, and 0.8 at $\Lambda = 0$ and 45 deg are shown in Tables 1 and 2, respectively. The modal participation values indicate that a 4-mode and a 10-mode model would yield accurate and convergent limit-cycle results for $\Lambda = 0$ and 45 deg, respectively. The modal convergence is further verified and confirmed by the convergence of the nondimensional dynamic pressure vs the number of modes in increasing frequency used in model reduction, as shown in Table 3.

Convergence of the LCO response using various finite element mesh sizes also is studied. Three mesh sizes of 8×8 (128 elements), 10×10 (200 elements), and 12×12 (288 elements) are used to model the simply supported square isotropic panel. Limit-cycle amplitude vs nondimensional dynamic pressure for the three mesh sizes at $\Lambda = 0$ and 45 deg are shown in Fig. 3. The maximum difference of the nondimensional dynamic pressure between the 8×8 and 12×12 models in Fig. 3 is less than 4%. Therefore, a 10×10 finite element mesh is used for the limit-cycle results in all of the examples presented.

The limit-cycle deflection for the simply supported square isotropic panel at amplitude of $w_{max}/h = 0.6$ for flow angles of $\Lambda = 0$ and 45 deg is shown in Figs. 4a and 4b, respectively. In both cases it is seen that the leading contour lines of the panel deflection are perpendicular to the flow direction and it is clear how the flow angle greatly changes the deflection shape.

The limit-cycle amplitude vs nondimensional dynamic pressure for $\Lambda = 0, 15, 30$, and 45 deg is given in Fig. 5. It is seen that increasing the flow angle has the effect of increasing the nondimensional

dynamic pressure at a fixed limit-cycle amplitude for this square isotropic panel. Figure 6 shows the effect of aspect ratio (a/b) on the nondimensional dynamic pressure at $\Lambda = 0$ and 45 deg. It is seen that, increasing the flow angle for isotropic panels with $(a/b) < 1$, the nondimensional pressure decreases at fixed limit-cycle amplitude.

C. Composite Panels

Flutter of (symmetric or antisymmetric) composite panels can be studied using the formulation and solution procedure presented. As an example, a simply supported rectangular graphite/epoxy panel of three layers [−40/40/−40] is investigated. The dimensions and material properties of the panel are as follows:

$$a = 15\,\text{in.}\,(38.1\,\text{cm}), \qquad b = 12\,\text{in.}\,(30.5\,\text{cm})$$

$$h = 0.048\,\text{in.}\,(0.122\,\text{cm}), \qquad E_1 = 22.5\,\text{Msi}\,(155\,\text{GPa})$$

$$E_2 = 1.17\,\text{Msi}\,(8.07\,\text{GPa}), \qquad G_{12} = 0.66\,\text{Msi}\,(4.55\,\text{GPa})$$

$$G_{23} = 0.44\,\text{Msi}\,(3.03\,\text{GPa}), \qquad \nu_{12} = 0.22$$

$$\rho = 0.1458 \times 10^{-3}\,\text{lb-s}^2/\text{in.}^4\,(1550\,\text{kg/m}^3)$$

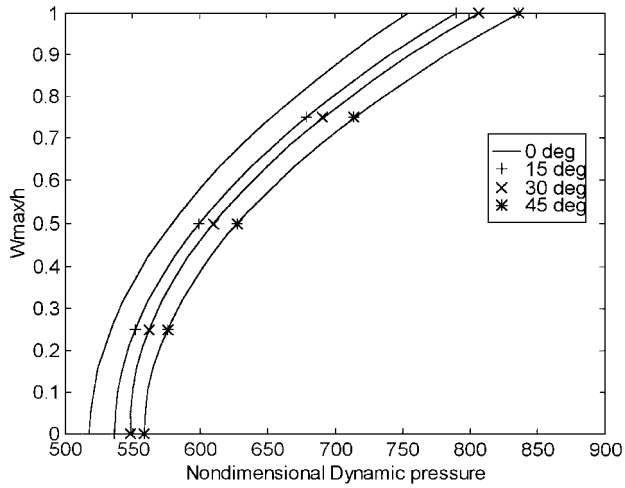

Fig. 5 Effect of flow yaw angle on nonlinear panel flutter for simply supported isotropic square panel.

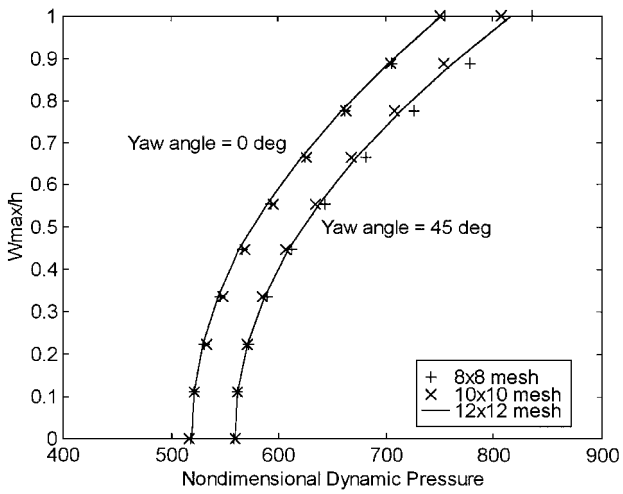

Fig. 3 Mesh convergence for isotropic square panel at different flow angles.

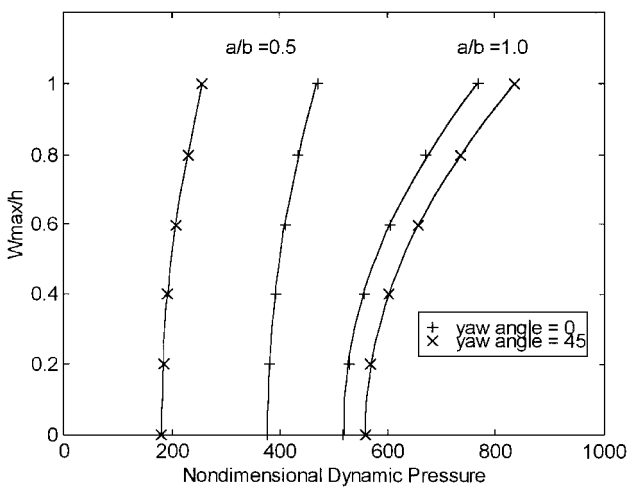

Fig. 6 Effect of panel aspect ratio on nonlinear panel flutter for simply supported isotropic square panel.

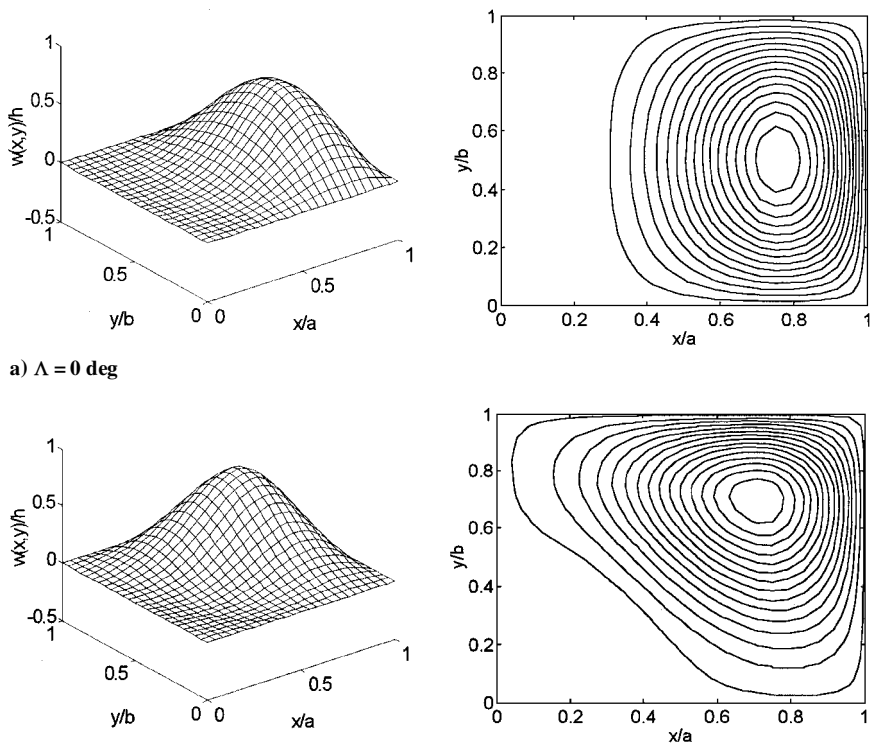

Fig. 4 Limit-cycle deflection for isotropic square simply supported panel at $w_{max}/h = 0.6$.

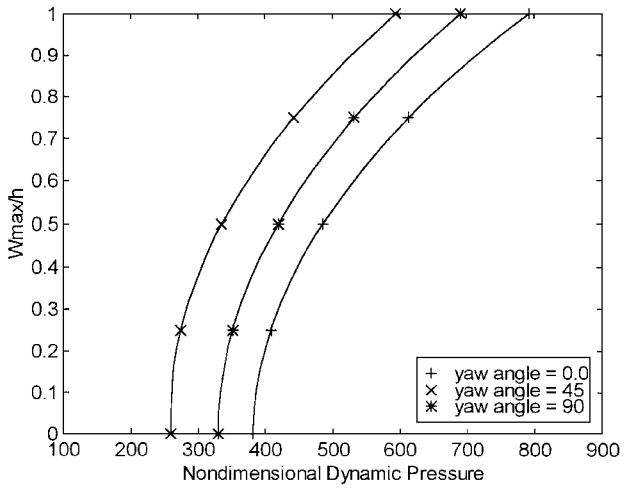

Fig. 7 Effect of flow yaw angle on nonlinear panel flutter for simply supported graphite/epoxy rectangular panel.

The complete plate is modeled using 10×10 mesh (200 MIN3 elements). The system equations in structure-node DOF are reduced to the modal coordinates using the lowest 16 modes in increasing-frequency order. The modal participation values for three limit-cycle amplitudes $w_{\max}/h = 0.01, 0.4$, and 0.8 at $\Lambda = 0$, 45, and 90 deg are shown in Tables 4, 5, and 6, respectively. These tables indicate that a 10-mode model would yield accurate and convergent limit-cycle results for all flow yaw angles. The modal convergence is further verified and confirmed by comparing the nondimensional dynamic pressure for different limit-cycle amplitudes using a 10-mode and a 16-mode model, as shown in Table 7.

The limit-cycle amplitude vs the nondimensional dynamic pressure for flow yaw angles of $\Lambda = 0$, 45, and 90 deg is shown in Fig. 7 for the rectangular composite panel. It is seen how the nondimensional dynamic pressure at 45-deg yaw angle is less than that of 0 and 90 deg at the same limit-cycle amplitude. The laminate considered is a good example to demonstrate the importance of the effect of the flow yaw angle on the nonlinear panel flutter. Figure 8 shows the panel limit-cycle deflection shape for $\Lambda = 0$, 45, and 90 deg. Unlike the isotropic case, the panel deflection for $\Lambda = 0$ and 90 deg is not symmetric about x or y axes, nor are the leading contour lines

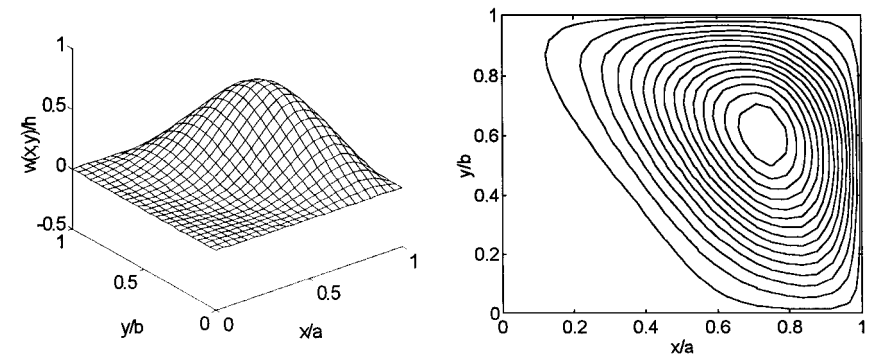

a) $\Lambda = 0$ deg

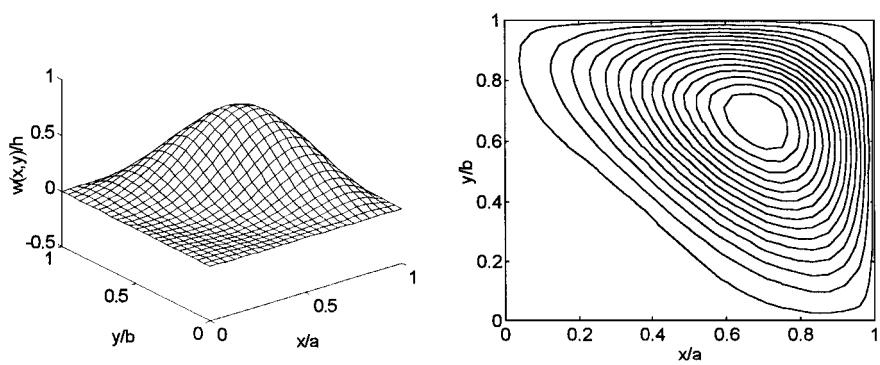

b) $\Lambda = 45$ deg

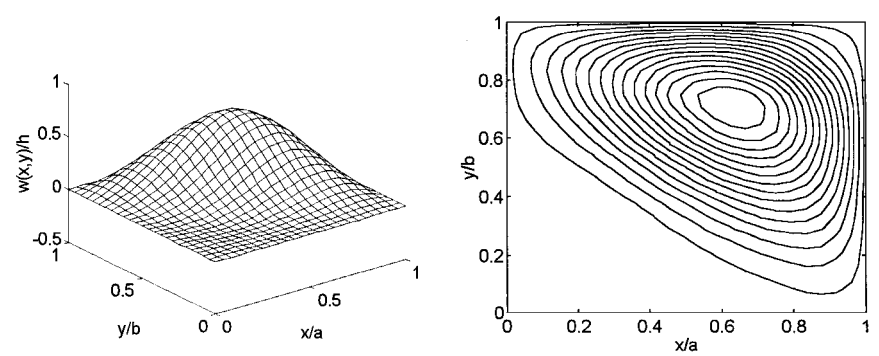

c) $\Lambda = 90$ deg

Fig. 8 Limit-cycle deflection for graphite/epoxy rectangular simply supported panel at $w_{\max}/h = 0.6$.

Table 4 Modal participation values at various limit-cycle amplitudes for a simply supported rectangular graphite/epoxy panel at 0-deg flow angle

	Modal participation, %															
w_{max}/h	q_1	q_2	q_3	q_4	q_5	q_6	q_7	q_8	q_9	q_{10}	q_{11}	q_{12}	q_{13}	q_{14}	q_{15}	q_{16}
0.01	25.12	37.26	4.95	14.98	4.88	4.41	1.36	1.60	1.34	1.31	0.69	0.16	0.29	1.10	0.56	0.01
0.4	24.99	35.37	5.86	14.49	4.87	4.70	1.68	1.54	1.65	1.50	0.68	0.37	0.34	1.26	0.60	0.11
0.8	23.52	31.85	8.07	13.65	4.98	5.18	2.56	1.41	2.17	1.90	0.67	0.76	0.50	1.72	0.70	0.36

Table 5 Modal participation values at various limit-cycle amplitudes for a simply supported rectangular graphite/epoxy panel at 45-deg flow angle

	Modal participation, %															
w_{max}/h	q_1	q_2	q_3	q_4	q_5	q_6	q_7	q_8	q_9	q_{10}	q_{11}	q_{12}	q_{13}	q_{14}	q_{15}	q_{16}
0.01	28.10	40.88	2.87	16.48	1.33	4.62	1.62	0.18	1.25	1.05	0.03	0.28	0.26	0.96	0.04	0.03
0.4	28.00	39.30	2.92	16.20	1.49	4.94	1.79	0.21	1.61	1.34	0.05	0.53	0.30	1.23	0.01	0.07
0.8	26.71	36.36	3.00	16.02	1.83	5.56	2.13	0.26	2.30	1.98	0.07	1.05	0.42	1.92	0.05	0.35

Table 6 Modal participation values at various limit-cycle amplitudes for a simply supported rectangular graphite/epoxy panel at 90-deg flow angle

	Modal participation, %															
w_{max}/h	q_1	q_2	q_3	q_4	q_5	q_6	q_7	q_8	q_9	q_{10}	q_{11}	q_{12}	q_{13}	q_{14}	q_{15}	q_{16}
0.01	24.03	35.15	8.57	13.48	5.86	3.45	3.03	1.54	0.61	1.26	0.63	0.18	0.79	0.98	0.33	0.09
0.4	24.56	32.85	9.60	12.68	5.96	3.58	3.42	1.53	0.84	1.49	0.64	0.38	0.92	1.15	0.39	0.01
0.8	22.50	29.37	11.44	12.05	6.38	3.98	4.48	1.53	1.28	1.97	0.67	0.80	1.20	1.59	0.57	0.19

Table 7 Nondimensional dynamic pressure at various limit-cycle amplitudes for a simply supported rectangular graphite/epoxy panel using 16 and 10 linear modes at $\Lambda = 0$, 45, and 90-deg

	Dynamic pressure λ at w_{max}/h					
Flow angle	Using 16 linear modes			Using 10 linear modes		
Λ	0.01	0.4	0.8	0.01	0.4	0.8
0	382	448	648	379	443	641
45	257	307	468	257	305	465
90	329	386	564	329	384	559

of the panel deflection perpendicular to the flow direction because this composite panel is not symmetric about the x or y axes.

IV. Conclusions

A finite element frequency-domain formulation is presented for the analysis of nonlinear flutter of composite panels at arbitrary flow yaw angle. The governing equations of motion are formulated by using the von Kármán large deflection, first-order transverse shear plate theories, and linear piston theory aerodynamics for arbitrary flow direction. A new and efficient solution procedure is presented by using the modal transformation to reduce the system equations in structure-node DOF to a set of a much smaller number of equations in the modal coordinates. The LUM/LTF approximate method then is used to solve the reduced nonlinear modal equations. The solution procedure has the advantage of using much less computational effort than solving the system equations of motion in the structure-node DOF. The effect of the flow yaw angle is studied for isotropic and composite panels. Results show that the flow yaw angle changes the shape of the limit-cycle deflection completely. It also shows that the effect of the yaw angle is a very important parameter, especially for composite panels, where the flow direction may increase or decrease the nondimensional dynamic pressure at fixed limit-cycle amplitude, depending on the panel lamination.

Appendix: Aerodynamic Matrices

The element DOF for the MIN3 elements are

$$\{w_e\}^T = \{w_b, w_m\}^T = \{w, \psi, w_m\}^T$$
$$= \{w_1, w_2, w_3, \psi_{x1}, \psi_{x2}, \psi_{x3}, \psi_{y1}, \psi_{y2}, \psi_{y3}, u_1, u_2, u_3, v_1, v_2, v_3\} \tag{A1}$$

The interpolation functions are given by[19,20]

$$w(x, y, t) = \lfloor H_w \rfloor \{w_b\} + \lfloor H_{w\psi} \rfloor \{\psi\}$$
$$\psi_x(x, y, t) = \lfloor H_{\psi x} \rfloor \{\psi\}, \qquad \psi_y(x, y, t) = \lfloor H_{\psi y} \rfloor \{\psi\}$$
$$u(x, y, t) = \lfloor H_u \rfloor \{w_m\}, \qquad v(x, y, t) = \lfloor H_v \rfloor \{w_m\} \tag{A2}$$

Element aerodynamic damping and mass matrices are given by

$$[m]_w = [g]_w = \int_A \{H_w\} \frac{D_{110}}{a^4} \lfloor H_w \rfloor \, dA$$
$$[m]_{w\psi} = [g]_{w\psi} = [g]_{\psi w}^T = \int_A \{H_w\} \frac{D_{110}}{a^4} \lfloor H_{w\psi} \rfloor \, dA$$
$$[m]_\psi = [g]_\psi = \int_A \{H_{w\psi}\} \frac{D_{110}}{a^4} \lfloor H_{w\psi} \rfloor \, dA$$
$$[g] = [m]_b = \begin{bmatrix} [g]_w & [g]_{w\psi} \\ [g]_{\psi w} & [g]_\psi \end{bmatrix} \tag{A3}$$

Element aerodynamic influence matrices are

$$([a_x]_w, [a_y]_w) = \int_A \frac{D_{110}}{a^3} \{H_w\} \left(\frac{\partial}{\partial x} \lfloor H_w \rfloor, \frac{\partial}{\partial y} \lfloor H_w \rfloor \right) dA$$
$$([a_x]_{w\psi}, [a_y]_{w\psi}) = \int_A \frac{D_{110}}{a^3} \{H_w\} \left(\frac{\partial}{\partial x} \lfloor H_{w\psi} \rfloor, \frac{\partial}{\partial y} \lfloor H_{w\psi} \rfloor \right) dA$$
$$([a_x]_\psi, [a_y]_\psi) = \int_A \frac{D_{110}}{a^3} \{H_{w\psi}\} \left(\frac{\partial}{\partial x} \lfloor H_{w\psi} \rfloor, \frac{\partial}{\partial y} \lfloor H_{w\psi} \rfloor \right) dA$$
$$([a_x], [a_y]) = \left(\begin{bmatrix} [a_x]_w & [a_x]_{w\psi} \\ [a_x]_{\psi w} & [a_x]_\psi \end{bmatrix}, \begin{bmatrix} [a_y]_w & [a_y]_{w\psi} \\ [a_y]_{\psi w} & [a_y]_\psi \end{bmatrix} \right) \tag{A4}$$

Acknowledgments

The first author would like to acknowledge support from the Aerospace Engineering Department, Old Dominion University. The second and third authors gratefully acknowledge the support by NASA Langley Research Center Contract NAS1-19858-94 and NAS1-19858-118.

References

[1]Kordes, E. E., and Noll, R. B., "Theoretical Flutter Analysis of Flat Rectangular Panels in Uniform Coplanar Flow with Arbitrary Direction," NASA TN D-1156, 1962.

[2]Bohon, H. L., "Flutter of Flat Rectangular Orthotropic Panels with Biaxial Loading and Arbitrary Flow Direction," NASA TN D-1949, 1963.

[3]Durvasula, S., "Flutter of Simply Supported, Parallelogrammic, Flat Panels in Supersonic Flow," *AIAA Journal*, Vol. 5, No. 9, 1967, pp. 1668–1673.

[4]Durvasula, S., "Flutter of Clamped Skew Panels in Supersonic Flow," *Journal of Aircraft*, Vol. 8, No. 6, 1971, pp. 461–466.

[5]Kariappa, V., Somashekar, B. R., and Shah, C. G., "Discrete Element Approach to Flutter of Skew Panels with In-Plane Forces Under Yawed Supersonic Flow," *AIAA Journal*, Vol. 8, No. 11, 1970, pp. 2017–2022.

[6]Sander, G., Bon, C., and Geradin, M., "Finite Element Analysis of Supersonic Panel Flutter," *International Journal for Numerical Methods in Engineering*, Vol. 7, No. 3, 1973, pp. 379–394.

[7]Shyprykevich, P., and Sawyer, J. W., "Orthotropic Panel Flutter at Arbitrary Yaw Angles—Experiment and Correlation with Theory," AIAA Paper 73-192, Jan. 1973.

[8]Sawyer, J. W., "Flutter of Elastically Supported Orthotropic Panels Including the Effects of Flow Angle," NASA TN D-7491, 1974.

[9]Bismarck-Nasr, M. N., "Finite Element Analysis of Aeroelasticity of Plates and Shells," *Applied Mechanics Reviews*, Vol. 45, No. 12, Pt. 1, 1992, pp. 461–482.

[10]Xue, D. Y., and Mei, C., "Finite Element Nonlinear Flutter and Fatigue Life of Two-Dimensional Panels with Arbitrary Temperatures in Supersonic Flow," *Journal of Aircraft*, Vol. 30, No. 6, 1993, pp. 993–1000.

[11]Xue, D. Y., "Finite Element Nonlinear Panel Flutter with Arbitrary Temperatures in Supersonic Flow," *AIAA Journal*, Vol. 31, No. 1, 1993, pp. 154–162.

[12]Dowell, E. H., "Panel Flutter: A Review of the Aeroelastic Stability of Plates and Shells," *AIAA Journal*, Vol. 8, No. 3, 1970, pp. 385–399.

[13]Gray, C. E., Jr., and Mei, C., "Large Amplitude Finite Element Flutter Analysis of Composite Panels in Hypersonic Flow," *Proceedings of the Dynamics Specialist Conference*, AIAA, Washington, DC, 1992, pp. 492–512.

[14]Zhou, R. C., Xue, D. Y., and Mei, C., "On Analysis of Nonlinear Panel Flutter at Supersonic Speeds," *First Industry/Academy Symposium on Research for Future Supersonic and Hypersonic Vehicles*, edited by A. Homaifar and J. C. Kelly, Jr., Vol. 1, TSI Press, Albuquerque, NM, 1994, pp. 343–348.

[15]Friedmann, P., and Hanin, M., "Supersonic Nonlinear Flutter of Orthotropic or Isotropic Panels with Arbitrary Flow Direction," *Israel Journal of Technology*, Vol. 6, No. 1–2, 1968, pp. 46–57.

[16]Chandiramani, N. K., Plaut, R. H., and Librescu, L., "Nonperiodic Flutter of Buckled Composite Panel," *Sadhana Journal*, Vol. 20, No. 2–4, 1995, pp. 671–689.

[17]Xue, D. Y., Wu, K., and Mei, C., "Iterative Real/Complex Eigen-solver and Parallel Processing for Nonlinear Panel Flutter," *Computing Systems in Engineering*, Vol. 5, No. 4–6, 1994, pp. 407–414.

[18]Xue, D. Y., Wu, K., and Mei, C., "Iterative Real/Complex Eigen-solver for Nonlinear Structural Vibrations," *Proceedings of the AIAA/ASME/ASCE/AHS/ASC 35th Structures, Structural Dynamics, and Materials Conference*, AIAA, Washington, DC, 1994, pp. 2343–2359.

[19]Tessler, A., and Hughes, T. J. R., "A Three-Node Mindlin Plate Element with Improved Transverse Shear," *Computer Methods in Applied Mechanics and Engineering*, Vol. 50, No. 1, 1985, pp. 71–91.

[20]Chen, R., "Finite Element Nonlinear Random Response of Composite Panels of Arbitrary Shape to Acoustic and Thermal Loads," Ph.D. Dissertation, Dept. of Aerospace Engineering, Old Dominion Univ., Norfolk, VA, May 1995.

[21]Zhou, R. C., Xue, D. Y., and Mei, C., "Finite Element Time Domain—Modal Formulation for Nonlinear Flutter of Composite Panels," *AIAA Journal*, Vol. 32, No. 10, 1994, pp. 2044–2052.

S. Saigal
Associate Editor